Dapagliflozin attenuates ferroptosis in diabetic nephropathy through activation of the Nrf2/HO-1 signaling pathway

HANSHUANG LIU[1], XIAOXIAO ZHANG[1], YUBING CUI[1], SHENGXI XIONG[1], LINJUAN HUANG[1], MIN LI[1], CHEN SHAO[2] and XIAOLEI HU[1]

[1]Department of Endocrinology, The First Affiliated Hospital of Bengbu Medical University, Bengbu, Anhui 233000, P.R. China; [2]Department of Endocrinology, The Second Affiliated Hospital of Bengbu Medical University, Bengbu, Anhui 233000, P.R. China

Received September 24, 2025; Accepted March 11, 2026

DOI: 10.3892/ijmm.2026.5842

Abstract. Renal tubular injury has emerged as a critical determinant in the pathogenesis of diabetic nephropathy (DN). Ferroptosis, a recently characterized mode of iron-dependent regulated cell death, has been implicated in the development of renal tubular damage. Dapagliflozin (DAPA), a sodium-glucose cotransporter 2 inhibitor, has demonstrated efficacy in attenuating DN progression and preserving renal function. The present study sought to elucidate the inhibitory mechanisms by which DAPA modulates ferroptosis in DN. To this aim, the expression profiles of key molecular markers within the ferroptosis cascade were systematically evaluated using 6-week-old male C57BL/6J mice and high-glucose-cultured human renal tubular epithelial cells as experimental models. The findings revealed that DAPA notably ameliorated renal histopathological alterations, upregulated the expression of solute carrier family 7 member 11, glutathione peroxidase 4 and ferritin heavy chain 1, whilst concomitantly downregulating transferrin receptor 1. These effects were mediated through the activation of nuclear factor erythroid 2-related factor 2 (Nrf2) and heme oxygenase-1 (HO-1) in C57BL/6J mice. Collectively, these data indicate that the reno-protective effects of DAPA in DN may be attributable to the suppression of ferroptosis via activation of the Nrf2/HO-1 signaling axis.

Introduction

Diabetic nephropathy (DN) constitutes one of the most serious microvascular complications of diabetes mellitus (DM), affecting 20-50% of diabetic patients and representing the predominant etiology of end-stage kidney disease (ESKD) requiring renal replacement therapy (1). The pathophysiology of DN is multifaceted, encompassing genetic susceptibility, perturbations in glucose metabolism, alterations in renal hemodynamics and the involvement of inflammatory mediators (2). According to the Joint Asian Diabetes Evaluation Program, the treatment and control rates of chronic kidney disease among Type 2 DM (T2DM) patients in China and several other Asian countries are suboptimal (3). Consequently, a comprehensive understanding of DN pathogenesis and the identification of novel therapeutic targets assumes paramount importance.

The kidney plays an indispensable role in maintaining systemic glucose homeostasis. Sodium-glucose cotransporter 2 (SGLT-2) inhibitors, including dapagliflozin (DAPA) and empagliflozin, have emerged as promising therapeutic agents for T2DM management (4). These pharmacological agents attenuate glucose reabsorption in the renal tubules through competitive inhibition of SGLT-2 proteins. SGLT-2 inhibition confers notable reno-protective effects, not only mitigating glomerular hyperfiltration but also reducing intraglomerular pressure through vasodilation of the efferent glomerular arterioles and vasoconstriction of the afferent arterioles (5). Beyond their primary glycemic benefits, SGLT-2 inhibitors also exert positive effects on multiple parameters, including improvements in blood lipids (6) and blood pressure (7), as well as reductions in uric acid levels (8). Furthermore, they demonstrate benefits in heart failure (9) and chronic kidney disease (10). In recent years, the advent of novel hypoglycemic agents has considerably expanded the therapeutic armamentarium for T2DM and DN. The DECLARE (11) and DAPA-CKD (12) studies have demonstrated that DAPA significantly improves renal outcomes and reduces the risk of adverse renal events in patients with T2DM, although the precise molecular mechanisms remain incompletely elucidated. Emerging evidence indicates that empagliflozin can attenuate ferroptosis in adriamycin-induced cardiotoxicity in non-diabetic mice, suggesting that SGLT-2 inhibitors may possess ferroptosis-modulatory properties (13). Nevertheless, the precise mechanisms underlying these effects warrant further investigation.

Ferroptosis represents a distinctive modality of regulated cell death that is morphologically, genetically and biochemically distinguishable from apoptosis, autophagy and necrosis. This process is predominantly characterized by perturbations

Correspondence to: Professor Xiaolei Hu, Department of Endocrinology, The First Affiliated Hospital of Bengbu Medical University, 801 Zhihuai Road, Bengbu, Anhui 233000, P.R. China
E-mail: huxiaolei@bbmc.edu.cn

Key words: ferroptosis, dapagliflozin, nuclear factor erythroid 2-related factor 2/heme oxygenase-1 signaling pathway, diabetic nephropathy, renal tubular injury

in iron homeostasis and excessive lipid peroxidation (14). The solute carrier family 7, member 11 (SLC7A11) serves a critical function in glutathione (GSH) biosynthesis by facilitating cystine transport into cells. Inhibition of SLC7A11 expression impairs GSH synthesis, compromises cellular antioxidant capacity and ultimately induces ferroptosis (15). Glutathione peroxidase 4 (GPX4), a central regulatory enzyme in ferroptosis, is indispensable for maintaining iron homeostasis through the degradation of lipid peroxides. GPX4 preserves the structural integrity of the membrane lipid bilayer by neutralizing lipid peroxides and mitigating their cytotoxicity. Inactivation of GPX4 results in the aberrant accumulation of lipid peroxides, thereby inducing ferroptosis (16). During ferroptosis, dysregulated expression of ferritin heavy chain 1 (FTH-1) and transferrin receptor 1 (TFR-1) culminates in ferrous iron accumulation, which drives the generation of reactive oxygen species (ROS) via the Fenton reaction (17). This surge in ROS overwhelms cellular antioxidant defenses, culminating in oxidative cell death. Malondialdehyde (MDA), a byproduct of lipid peroxidation, readily forms adducts with proteins and DNA, causing significant cytotoxic effects and inducing ferroptosis (18). The kidney, replete with mitochondria, exhibits heightened vulnerability to oxidative stress, suggesting a mechanistic link between ferroptosis and DN. A study has documented iron overload and ROS accumulation in the kidneys of diabetic mice and human renal proximal tubule cells cultured under high glucose (HG) conditions (19). Ferroptosis has also been implicated in renal pathologies such as acute renal failure, renal ischemia-reperfusion injury (IRI) and DN (20-22). These findings underscore the pivotal role of ferroptosis in the progression of renal injury in DN, intimating that targeting ferroptosis might offer a viable therapeutic strategy. However, the precise molecular mechanisms underlying ferroptosis in DN remain to be comprehensively elucidated.

Iron accumulation and lipid peroxidation constitute the main characteristics of ferroptosis, with a series of genes governing the antioxidant system, iron homeostasis and lipid metabolism orchestrating this cell death modality. Nuclear factor erythroid 2-related factor 2 (Nrf2), a crucial transcription factor combating oxidative stress, orchestrates the expression of antioxidant enzymes and regulates iron metabolism, making inhibition of Nrf2 a potential enhancer of ferroptosis sensitivity (23). Heme oxygenase-1 (HO-1), known for its potent antioxidant and cytoprotective properties, is instrumental in preserving cellular redox equilibrium and counteracting oxidative stress (24). Numerous studies have underscored the protective effects of Nrf2/HO-1 upregulation against oxidative stress (25-27), inextricably linking this pathway with ferroptosis regulation (28-30). Research has demonstrated that trehalose can impede ferroptosis via the Nrf2/HO-1 pathway, promoting functional recovery in mice with spinal cord injuries (31). Additionally, cetuximab has been shown to potentiate RSL3-induced ferroptosis by inhibiting the Nrf2/HO-1 signaling pathway in KRAS-mutant colorectal cancer (32). As our comprehension of ferroptosis and its associated mechanisms deepens, the pivotal role of the Nrf2/HO-1 signaling pathway in mediating this process becomes increasingly apparent. A study has indicated that DAPA can mitigate diabetic tubular injury by inhibiting ferroptosis (33) and Zhang *et al* (34) further suggested that pathways such as Nrf2 signaling may be involved. Building on these findings, the present study specifically investigated the role of the Nrf2/HO-1 signaling pathway in mediating the anti-ferroptotic effects of DAPA. This was achieved by observing ferroptosis in HG-induced human renal tubular epithelial cells (HK-2) *in vitro* and in a mouse model of DN *in vivo*. The present investigation may offer a fresh perspective on the mechanism of DAPA in treating DN.

Materials and methods

Animal experiment. The present study used a total of 30 male pathogen-free C57BL/6J mice (6 weeks old, weighing 19-22 g) procured from Sipeifu (Beijing) Biotechnology Co., Ltd. The mice were maintained in cages under controlled environmental conditions (temperature: 20±2˚C; 12-h light/dark cycle; humidity: 55±10%) with *ad libitum* access to standard chow and water. All animal experiments and research procedures were approved by the Clinical Medical Research Ethics Committee of the First Affiliated Hospital of Bengbu Medical University [Bengbu, China; approval no. (2023) No. 592]. Following acclimatization, all mice were fed a standard diet for 1 week. Subsequently, 5 mice were randomly designated as the normal control group (NC group) and continued on the standard diet. The remaining animals were administered a high-fat diet [HFD; Sipeifu (Beijing) Biotechnology Co., Ltd.; composition: 67% maintenance feed for mice and rats, 10% lard, 20% sucrose, 2.5% cholesterol and 0.5% sodium cholate] for 4 weeks, followed by intraperitoneal administration of low-dose streptozotocin (STZ; 50 mg/kg, dissolved in 1% citric acid buffer, pH 4.2) over 3 consecutive days. Mice in the NC group received an equivalent volume of citrate buffer vehicle. A total of 3 days after the final STZ injection, blood glucose concentrations were monitored from tail vein samples using a glucometer. The collected blood volume was ~0.5 μl and samples were collected from all mice. Mice with random blood glucose concentrations >16.7 mmol/l for 3 consecutive days were continued on the HFD for an additional 8 weeks. In total, 5 mice in the normal group did not reach this threshold (as expected), while all 25 mice in the other groups reached this threshold. The DN model was considered to have been successfully established in mice demonstrating positive urinary protein. The HFD mice were then randomly divided into five groups (all n=5): i) The DN control group, which received daily saline injections; ii) the DAPA group, which received daily oral gavage of DAPA (10 mg/kg/day; AstraZeneca); iii) the DN + small interfering (si)-NC group (si-NC group), which received tail vein injections of si-NC (5 nmol/20 g) every 3 days; iv) the DN + si-Nrf2 group (si-Nrf2 group), which received tail vein injections of si-Nrf2 (5 nmol/20 g) every 3 days; and v) the DN + si-Nrf2 + DAPA group (si-Nrf2 + DAPA group), which received tail vein injections of si-Nrf2 (5 nmol/20 g) every 3 days and daily oral gavage of DAPA (10 mg/kg/day) for 8 weeks. The siRNA sequences (Shanghai GenePharma Co., Ltd.) are listed in Table I.

Conducted in accordance with the relevant institutional animal experiment protocols and the GB/T 39760-2021 Guidelines for the Humane Euthanasia of Experimental Animals, researchers monitored the overall health and behavior

Table I. siRNA sequences for transfection (*Mus musculus*).

siRNA	Sense sequences (5'-3')	Antisense sequences (5'-3')
si-Nrf2	GAGGAUGGAAAGCCUUACUTT	AGUAAGGCUUUCCAUCCUCTT
si-NC	UUCUCCGAACGUGUCACGUTT	ACGUGACACGUUCGGAGAATT

si, small interfering; Nrf2, nuclear factor erythroid2-related factor 2; NC, normal control.

of the laboratory mice daily during the experiment and detailed assessments at least twice a week, including measurements of body weight, food intake, water intake and blood glucose. The humane endpoints for early euthanasia included: i) Inability to eat or drink; ii) persistent lethargy, inability to walk or inability to maintain normal posture; iii) difficulty breathing; or iv) other severe conditions determined by the animal center staff that require early termination. In the present study, no animals reached these humane endpoints before the planned endpoint. At week 23, mice were anesthetized with an intraperitoneal injection of 0.3% pentobarbital sodium (30 mg/kg) and blood was collected via cardiac puncture. The mice were euthanized by cervical dislocation prior to mortality and the loss of respiration and reflexes were confirmed before tissue collection. The kidneys were collected, with some tissue fixed in 4% paraformaldehyde, placed at room temperature and used for histological analysis within a week. The remaining tissue was washed three times with PBS, quickly frozen in liquid nitrogen and then stored at -80˚C for subsequent molecular analysis.

Biochemical measurements. Individual mice were housed in metabolic cages for 24 h. Urine was collected at weeks 5 and 15 and the urine volume was measured. The urine samples were centrifuged at 4˚C, 1,000 x g for 20 min to obtain the supernatant and the concentrations of urinary albumin and creatinine were determined using a mouse Mau ELISA kit (Wuhan Elabscience Biotechnology Co., Ltd.; cat. no. E-EL-M0792) and a mouse Cr ELISA kit (Wuhan Elabscience Biotechnology Co., Ltd.; cat. no. E-EL-0058), respectively. The urinary albumin-to-creatinine ratio (ACR) was then calculated. At week 23, blood samples were collected and centrifuged at 4˚C, 3,000 x g for 5 min to obtain plasma for the determination of blood creatinine levels.

Histological evaluation and immunohistochemistry. Kidney tissues were fixed in 4% paraformaldehyde at room temperature for 1 week, embedded in paraffin and sectioned into 4-μm-thick slices. For HE staining, tissue sections were deparaffinized in xylene I and II for 10 min each, then sequentially hydrated for 5 min each in xylene/ethanol (1:1), 100% ethanol I/II and 80% ethanol, followed by rinsing with tap water. Hematoxylin staining was performed for 5 min, followed by washing with tap water, differentiation in 1% hydrochloric acid for 30 sec and bluing under running tap water. Eosin staining was carried out for 1 min, followed by rinsing under running water. Then, the sections were dehydrated through a graded series of 95% ethanol I/II and 100% ethanol I/II for 5 min each, treated with xylene I and II for 5 min each, cleared in xylene three times (3 min each), mounted with neutral resin and observed under a microscope.

For Masson staining, the steps for deparaffinization and hydration of the slices were the same as HE staining. The sections were stained with hematoxylin for 5 min, rinsed with distilled water, differentiated with acidic differentiation solution for 30 sec, rinsed with tap water for 10 min and quickly rinsed with distilled water. The sections were then stained with Acid Fuchsin staining solution for 10 min, quickly rinsed with distilled water, then differentiated with phosphomolybdic acid differentiation solution for 2 min. The differentiation solution was discarded and bright green staining solution was added for 1 min. The samples were quickly rinsed with distilled water, differentiated with acidic differentiation solution for 1 min, quickly dehydrated through a graded ethanol series (70, 80, 90 and 100% for 10 sec each), cleared three times with xylene (5 min each), mounted with neutral resin and observed under a microscope.

For periodic acid-Schiff (PAS) staining, the steps for deparaffinization and hydration of tissue sections were the same as HE staining. The sections were oxidized at room temperature in iodine solution for 10 min, then washed with distilled water for 5 min. Schiff's reagent was added and incubated in a dark box at 37˚C for 1 h, followed by washing with distilled water for 5 min. Subsequently, the sections are counterstained with hematoxylin for 3 sec, differentiated with hydrochloric acid for 30 sec, rinsed twice with tap water and blued for 5 min. Finally, the sections underwent graded dehydration, xylene clearing and mounting with neutral resin as in routine HE staining, then observed and imaged under the microscope.

For immunohistochemistry, after dewaxing and hydration, the sections were incubated with 3% hydrogen peroxide-methanol solution at room temperature for 15 min to quench endogenous peroxidase activity and 1 mmol/l levamisole for 20 min to inhibit endogenous alkaline phosphatase activity. Antigen retrieval was performed with citrate and the samples were blocked with 10% goat serum (Beyotime Biotechnology) for 30 min at 37˚C. The kidney sections were then incubated overnight at 4˚C with the following primary antibodies: Anti-Nrf2 (1:500; cat. no. 80593-1-RR; Wuhan Sanying Biotechnology), anti-HO-1 (1:500; cat. no. 81281-1-RR; Wuhan Sanying Biotechnology), anti-GPX4 (1:100; cat. no. 14432-1-AP; Wuhan Sanying Biotechnology), anti-SLC7A11 (1:100; cat. no. 26864-1-AP; Wuhan Sanying Biotechnology), anti-FTH-1 (1:100; cat. no. DF6278; Affinity Biosciences) and anti-CD71/TFR-1 (1:2,000; cat. no. 10084-2-AP; Wuhan Sanying Biotechnology). Following washing with PBS, secondary antibodies (1:500; cat. nos. 31430 and 31466; Thermo Fisher Scientific, Inc.) were

Table II. siRNA sequences for cell transfection (*Homo sapiens*).

siRNA	Sense sequences (5'-3')	Antisense sequences (5'-3')
si-Nrf2	GACAGAAGUUGACAAAUUAUTT	AUAAUUGUCAACUUCUGUCTT
si-NC	UUCUCCGAACGUGUCACGUTT	ACGUGACACGUUCGGAGAATT

si, small interfering; Nrf2, nuclear factor erythroid2-related factor 2; NC, normal control.

applied and incubated at room temperature for 30 min. After further washing with PBS, the DAB chromogenic kit was used for color development. After counterstaining with hematoxylin (10 min at room temperature) and dehydration with an ethanol gradient, the sections were finally sealed with xylene. Images of the sections were captured under a light microscope. Aperio ImageScope (v12.4.0.7000; Leica Biosystems) was used for positive area quantification.

Transfection. When the cells in a 6-well plate reached 65-75% confluency, si-NC or si-Nrf2 (Shanghai GenePharma Co., Ltd.) and Lipofectamine 2000 transfection reagent (Invitrogen; Thermo Fisher Scientific, Inc.) were separately mixed with Opti-MEM serum-reduced medium (Invitrogen; Thermo Fisher Scientific, Inc.). After standing for 5 min, the mixtures were combined and allowed to stand for an additional 20 min before being added to the 6-well plate. Following transfection for 6 h, the medium was replaced, DAPA at a concentration of 25 μmol/l was added for another 48 h. Transfection efficiency was confirmed by reverse transcription-quantitative PCR (RT-qPCR) and western blotting (WB). The siRNA sequences are listed in Tables I and II.

Cell culture. HK-2 cells were procured from The Cell Bank of Type Culture Collection of The Chinese Academy of Sciences. Cells in the NC group were cultured in complete DMEM containing 5.5 mmol/l glucose (Shanghai BasalMedia Technologies Co., Ltd.), 10% high-grade fetal bovine serum (FBS; Shanghai ExCell Biology, Inc.) and a penicillin-streptomycin solution (100X; Biosharp Life Sciences). The HG group cells were cultured in DMEM containing 25 mmol/l glucose (Shanghai BasalMedia Technologies Co., Ltd.), 10% FBS and penicillin-streptomycin solution (100X). The ferroptosis activator group (erastin group) was cultured in medium containing 5.5 mmol/l glucose + 2.5 μmol/l erastin for 48 h. The HG + DAPA group (DAPA group) was cultured in medium containing 25 mmol/l glucose for 48 h, with the addition of DAPA at a final concentration of 25 μmol/l for another 48 h. The HG + ferrostatin-1 (Fer-1) group (Fer-1 group) was cultured in medium containing 25 mmol/l glucose for 48 h, with the addition of a ferroptosis inhibitor at a final concentration of 1 μmol/l for another 48 h. The HG + si-NC group (si-NC group) was cultured in medium containing 25 mmol/l glucose for 48 h, with the addition of 5 μl of si-NC at a concentration of 20 μM for 6 h, followed by culture in medium containing 5.5 mmol/l glucose for 48 h. The HG + si-Nrf2 group (si-Nrf2 group) was cultured in medium containing 25 mmol/l glucose for 48 h, with the addition of 5 μl of si-Nrf2 at a concentration of 20 μM for 6 h, followed by culture in medium containing 5.5 mmol/l glucose for 48 h. The HG + si-Nrf2 + DAPA group (si-Nrf2 + DAPA group) was cultured in medium containing 25 mmol/l glucose for 48 h, with the addition of 5 μl of si-Nrf2 at a concentration of 20 μM for 6 h, followed by culture in medium containing DAPA at a final concentration of 25 μmol/l for 48 h. All cells were cultured in an incubator at 37˚C with 5% CO. The siRNA sequences (Shanghai GenePharma Co., Ltd) are listed in Table II.

Cell viability assay. Cell viability was assessed using the Cell Counting Kit-8 (CCK-8; Beyotime Biotechnology) following the manufacturer's instructions. Cells were seeded in 96-well plates at a density of 5,000 cells (100 μl) per well, incubated at 37˚C for 24 h and then treated with varying concentrations of the test substances (DAPA, Fer-1 and erastin) for specified durations (such as 24, 48 and 72 h). After treatment, 10 μl of the CCK-8 working reagent was added to each well and incubated for 2 h at 37˚C. The absorbance at 450 nm was measured using a Multifunctional microplate reader (Ensight; PerkinElmer, Inc.).

Determination of iron and MDA. Collected cells and appropriately sized tissues (Iron Test Kit: 0.1 g of fresh tissue block per 0.9 ml of reagent; MDA Test Kit: The tissue weight was 10% of the homogenate or lysis solution) were homogenized in buffer or lysate, thoroughly mixed and placed on ice for 10 min for lysis. The homogenates were then centrifuged at 4˚C, 15,000 x g for 10 min and the resulting supernatants were collected for analysis. The iron and MDA concentrations were determined using an Iron assay kit (Wuhan Elabscience Biotechnology Co., Ltd.) and a trace MDA assay kit (Beyotime Biotechnology), respectively. Working reagents were prepared as per the manufacturer's instructions. Subsequently, the samples were added to a 96-well plate with the working reagents and incubated at 37˚C for 10 min. The absorbance values of each well were measured at 593 nm (iron assay) and 532 nm (MDA assay) using a spectrophotometer. The concentrations of iron and MDA were calculated according to the manufacturer's instructions.

Measurement of ROS production. Intracellular levels of ROS were assessed using 2',7'-dichlorofluorescein diacetate (Beyotime Biotechnology). Method 1: Cells cultured in 6-well plates were incubated with 10 μmol/l of 2',7'-dichlorofluorescein diacetate in a cell culture incubator at 37˚C, shielded from light, for 1 h. After washing, the cells were trypsinized, collected, resuspended in PBS and the fluorescence intensity was measured using a flow cytometer (FACSCanto; BD Biosciences) with an excitation wavelength of 488 nm and an

Table III. PCR primer sequences (*Homo sapiens*).

Gene	Forward primer sequences (5'-3')	Reverse primer sequences (5'-3')
Nrf2	ACGGTATGCAACAGGACATTGAGC	GGAAGTCGTCGTAGGAGAGGTGT
HO-1	AAGACTGCGTTCCTGCTCAAC	GCTGTCAACGACATCCCGAAA
GPX4	GAGGCAAGACCGAAGTAAACTAC	AAGGGCACATTGGTCAAGCC
SLC7A11	CCCAGATATGCATCGTCCTT	ATACCCTGTTCTTTGGGTCC
FTH-1	CCCCCATTTGTGTGACTTCAT	TTACTTTCGATTCGGAGCCCG
TFR-1	GGACGCGCTAGTGTTCTTCT	GGACCGAGCCGTTCATCTAC
GAPDH	ACCCAGAAGACTGTGGATGG	GTTCCAGTAGGGACTCGACT

Nrf2, nuclear factor erythroid2-related factor 2; HO-1, heme oxygenase-1; GPX4, glutathione peroxidase 4; SLC7A11, solute carrier family 7, member 11; FTH-1, ferritin heavy chain 1; TFR-1, transferrin receptor 1.

Table IV. PCR primer sequences (*Mus musculus*).

Gene	Forward primer sequences (5'-3')	Reverse primer sequences (5'-3')
Nrf2	GCATAGAGCAGGACATGGAGCA	GGAAGGAGGCGACGGTAGTCA
HO-1	AAGCCGAGAATGCTGAGTTCA	AGGAACATGGTATAGATGTGCCG
GPX4	CAGGAGCCAGGAAGTAAT	GAGTAACTATTCTTGCCGAC
SLC7A11	CCTCTGACGATGGTGATGCTCTTC	GAAATGAGCCTGGGTAAGTCGTGG
FTH-1	TGCCATCAACCGCCAGATCAA	CTGACCCTCTCGCCCGACTTA
TFR-1	GTTTCCGCCATCTCAGTCATCAGG	GACCACAACGCCGCTTCAGG
GAPDH	CCCACTAACATCAAATGGGG	TTGAAACCGTAACACCTTCC

Nrf2, nuclear factor erythroid2-related factor 2; HO-1, heme oxygenase-1; GPX4, glutathione peroxidase 4; SLC7A11, solute carrier family 7, member 11; FTH-1, ferritin heavy chain 1; TFR-1, transferrin receptor 1.

emission wavelength of 525 nm. The results were analyzed using FlowJo (v10; FlowJo LLC) Method 2: Cells cultured in 6-well plates were incubated with 10 μmol/l of 2',7'-dichlorofluorescein diacetate in a 37˚C cell culture incubator, protected from light, for 1 h. After washing, the cells were further incubated with DAPI staining solution for 20 min at 37˚C. The staining solution was then removed and the cells were washed three times with PBS. The cells were visualized using a fluorescence imaging microscopy system (Axio Vert AI; Zeiss GmbH).

RT-qPCR. Total RNA from kidney tissues and HK-2 cells was extracted and purified using Universal Total RNA Isolation Reagent (Biosharp Life Sciences). After quantifying the concentration and purity of the RNA, 1 μg of RNA was reverse transcribed into 20 μl of cDNA using HiScript II Q RT SuperMix for qPCR (Vazyme Biotech Co., Ltd.) at 50˚C for 15 min and 85˚C for 5 sec. The cDNA samples were amplified using a SYBR Green fluorescent PCR kit (Vazyme Biotech Co., Ltd.) on a fluorescence qPCR instrument (QuantStudio DX; Applied Biosystems; Thermo Fisher Scientific, Inc.). PCR was performed in triplicate with the following thermocycler profile: Denaturation at 95˚C for 5 min; 95˚C, 10 sec and 60˚C, 30 sec for 40 cycles of amplification. The relative abundance of the target genes was normalized to GAPDH using the $2^{-\Delta\Delta Cq}$ method (35). PCR primer sequences are provided in Tables III and IV.

Transmission electron microscopy. HK-2 cell pellets were collected and fixed in 2.5% glutaraldehyde (Wuhan Servicebio Technology Co., Ltd.; cat. no. G1102) at 4˚C for >2 h, then washed three times with 0.1 M phosphate buffer for 15 min each. After fixation with 1% osmium acid solution at room temperature for 1.5 h, the samples were washed three times with 0.1 M phosphate buffer and gradually dehydrated in ethanol (50-100%). The samples were embedded the samples and cured at 60˚C for 48 h. A microtome was used to cut the embedded samples into 60 nm ultrathin sections, which were then stained with 2% uranyl acetate at room temperature in the dark for 20 min and lead citrate at room temperature for 10 min. In total, three samples were prepared per group and five random fields of view were selected for each sample for observation and imaging under a transmission electron microscope.

WB analysis. Kidney tissues and cells were lysed with Western and IP lysis solution (Beyotime Biotechnology) containing 1% protease inhibitor for 30 min. The lysates were then centrifuged at 4˚C and 12,000 x g for 25 min to collect the supernatant. After quantification using the BCA protein assay kit, sampling buffer was added to the supernatant, which was mixed and boiled for 10 min. Proteins (cell sample: 20-30 μg per well; tissue sample: 30-50 μg per well) were separated by electrophoresis on a 10% SDS-polyacrylamide gel and transferred to

a PVDF membrane. The membrane was washed three times with TBST (0.1% Tween) buffer, sealed with protein-free rapid closure solution (Shanghai Baibo Biotechnology Co., Ltd.) at room temperature for 30 min, washed three times again and then incubated with the primary antibodies on a shaker at 4˚C overnight. The following primary antibodies were used: Anti-Nrf2 (1:1,000; cat. no. 80593-1-RR; Wuhan Sanying Biotechnology), anti-HO-1 (1:5,000; cat. no. 81281-1-RR; Wuhan Sanying Biotechnology), anti-GPX4 (1:2,000; cat. no. 14432-1-AP; Wuhan Sanying Biotechnology), anti-SLC7A11 (1:1,000; cat. no. 26864-1-AP; Wuhan Sanying Biotechnology), anti-FTH-1 (1:1,000; cat. no. DF6278; Affinity Biosciences), anti-CD71/TFR-1 (1:5,000; cat. no. 10084-2-AP; Wuhan Sanying Biotechnology) and anti-GAPDH (1:1,000; cat. no. GB11002; Wuhan Servicebio Technology Co., Ltd.). After washing the membrane three times, it was incubated with an HRP-labeled secondary antibody (10,000; cat. no. 45468; Shanghai Xitang Biotechnology Co., Ltd.) at room temperature for 2 h. The protein bands were then visualized using enhanced chemiluminescence reagents and semi-quantified in ImageJ software (version 1.54p; National Institutes of Health).

Statistical analysis. Statistical analyses were conducted using GraphPad Prism 8.0 software (Dotmatics). Values are shown as the mean ± SD. For multiple group comparisons, one-way ANOVA followed by Tukey's multiple comparisons test was performed. When two groups were compared, an unpaired t-test was used. Statistical significance was defined as $P<0.05$.

Results

Ferroptosis occurs in HK-2 cells cultured with HG. In the present study, HK-2 cells treated with 5.5 mmol/l glucose served as the NC group, while those cultured with 25 mmol/l glucose represented the HG group. The cell viability in HG medium with varying concentrations of DAPA (0, 3.125, 6.25, 12.5, 25, 37.5, 50 and 100 μmol/l) was evaluated at specific time points. Notably, a peak in cell viability was observed at 25 μmol/l of DAPA, followed by a decline with further increases in concentration (Fig. 1A). As Fer-1 and erastin were used as controls in subsequent experiments, the optimal concentrations of these reagents were also tested. Treatment with different concentrations of Fer-1 for 48 h resulted in increased cell viability across all Fer-1-treated groups, with the highest viability noted at 1 μmol/l (Fig. 1B). Similarly, after 48 h of exposure to varying concentrations of erastin, cell viability decreased in all erastin-treated groups, reaching its lowest point at 2.5 μmol/l (Fig. 1C).

To elucidate the manifestation of ferroptosis in HG-stimulated HK-2 cells, the mRNA expression levels of GPX4 (Fig. 1D), SLC7A11 (Fig. 1E), FTH-1 (Fig. 1F) and TFR-1 (Fig. 1G) were examined using RT-qPCR. Compared with the NC group, the HG group exhibited decreased mRNA expression of GPX4, SLC7A11 and FTH-1, alongside increased expression of TFR-1. Ultrastructural analysis revealed morphological characteristics indicative of ferroptosis in the HG and erastin cell groups, such as mitochondrial contraction, increased membrane density and reduced or absent mitochondrial ridges (Fig. 1H). Furthermore, intracellular ROS levels were measured using fluorescent probes. The HG and erastin groups exhibited a notable rightward shift in the peak fluorescence value compared with the NC group, indicating a higher degree of fluorescence production (Fig. 1I and J). Additionally, MDA and iron content were assessed using colorimetric assays, revealing a 33% increase in MDA production (Fig. 1K) and a 35% increase in iron content (Fig. 1L) in the HG and erastin groups compared with the NC group. The expression levels of ferroptosis-related proteins in each group were also investigated using WB. The protein expression patterns of GPX4, SLC7A11, FTH-1 and TFR-1 were consistent with the changes observed in the corresponding RT-qPCR assay (Fig. 1M and N). These findings highlight the alignment of ferroptosis-related alterations in the HG group with those in the erastin group.

DAPA alleviates HG-induced ferroptosis in HK-2 cells. To delve deeper into the impact of DAPA on HG-induced ferroptosis in HK-2 cells, RT-qPCR was conducted to assess the mRNA expression levels in each group. Notably, compared with the HG group, DAPA and Fer-1 treatment improved the decreased expression of GPX4 (Fig. 2A), SLC7A11 (Fig. 2B) and FTH-1 (Fig. 2C), while inhibiting the increased expression of TFR-1 (Fig. 2D) in HK-2 cells exposed to HG. Furthermore, DAPA and Fer-1 treatment led to a reduction in ROS (Fig. 2E and F), MDA (Fig. 2G) and iron content (Fig. 2H) under ferroptosis conditions, indicating its potential to mitigate ferroptosis-induced damage in HK-2 cells. Additionally, at the protein level, DAPA and Fer-1 reversed the expression patterns of ferroptosis-related genes. In the HG group, the decreased expression of GPX4, SLC7A11 and FTH-1 was rescued by DAPA, while the increase of TFR-1 was inhibited by DAPA (Fig. 2I and J). These findings demonstrate that DAPA exerts a protective effect against ferroptosis in HK-2 cells. Notably, the observed changes in ferroptosis-related markers in the DAPA group were consistent with those in the Fer-1 group.

DAPA activates the Nrf2/HO-1 signaling pathway in HG-induced HK-2 cells. Recognizing the pivotal role of Nrf2 in oxidative stress and ferroptosis, the impact of DAPA on Nrf2/HO-1 signaling was next investigated. RT-qPCR analysis revealed that the Nrf2 and HO-1 mRNA levels were downregulated in the HG group, whereas DAPA treatment mitigated these alterations (Fig. 3C and D). Furthermore, WB results corroborated these findings, showing a decrease in Nrf2 and HO-1 protein levels in HK-2 cells exposed to HG, which were restored upon DAPA treatment (Fig. 3A and B). To deepen our understanding of the interplay between Nrf2/HO-1 and ferroptosis, Nrf2 knockdown experiments were conducted. RT-qPCR (Fig. 3E-J) and WB (Fig. 3O and P) analyses revealed that knockdown of Nrf2 led to a decrease in the expression of Nrf2, HO-1, GPX4, SLC7A11 and FTH-1, and an increase in the expression of TFR-1. However, administration of DAPA under the same conditions attenuated these effects. Additionally, Nrf2 knockdown showed an inhibitory effect on the reduction of MDA, iron content and ROS compared with the DAPA treatment group (Fig. 3K-N). These findings suggest that DAPA may alleviate the damage caused by ferroptosis in HK-2 cells by upregulating the Nrf2/HO-1 signaling pathway.

Modeling process and characteristic changes in DN mice. To further validate the findings, *in vivo* experiments were

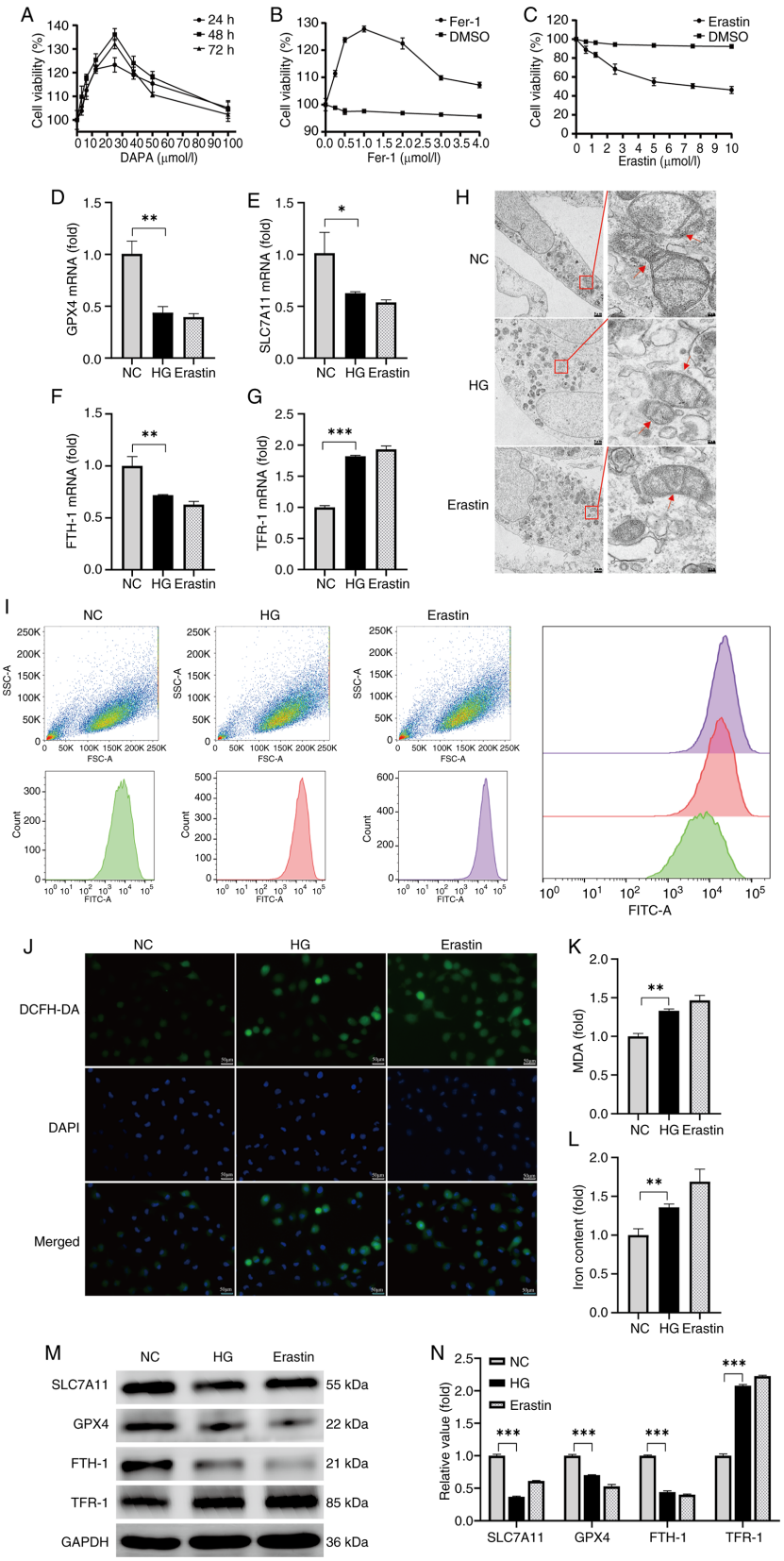

Figure 1. Expression of genes associated with ferroptosis was assessed in HK-2 cells exposed to HG. (A) Cell viability was measured after incubation with varying concentrations of DAPA for 24, 48 and 72 h. Similarly, cell viability was evaluated after treatment with different concentrations of (B) Fer-1 or (C) erastin for 48 h. The mRNA levels of (D) GPX4, (E) SLC7A11, (F) FTH-1 and (G) TFR-1 were determined in each cell group. (H) Transmission electron microscopy was employed to examine mitochondrial morphology in cells from the NC, HG and erastin treatment groups. (I) Levels of ROS were assessed in each group, (J) with green representing ROS and blue representing the nucleus in the representative images. (K) MDA and (L) cellular iron content measurements were also conducted. (M) The protein levels of GPX4, SLC7A11, FTH-1 and TFR-1 were analyzed via immunoblotting in cells from the NC, HG and erastin groups, (N) with semi-quantitative analysis of the immunoblotting results shown. The bars indicate the mean ± SD from three independent experiments. *P<0.05, **P<0.01, ***P<0.001 compared with the normal group. ROS, reactive oxygen species; MDA, malondialdehyde; HG, high glucose; NC, normal control; DAPA, dapagliflozin; Fer-1, ferrostatin-1; GPX4, glutathione peroxidase 4; SLC7A11, solute carrier family 7, member 11; FTH-1, ferritin heavy chain 1; TFR-1, transferrin receptor 1; DCFH-DA, 2',7'-dichlorodihydrofluorescein diacetate.

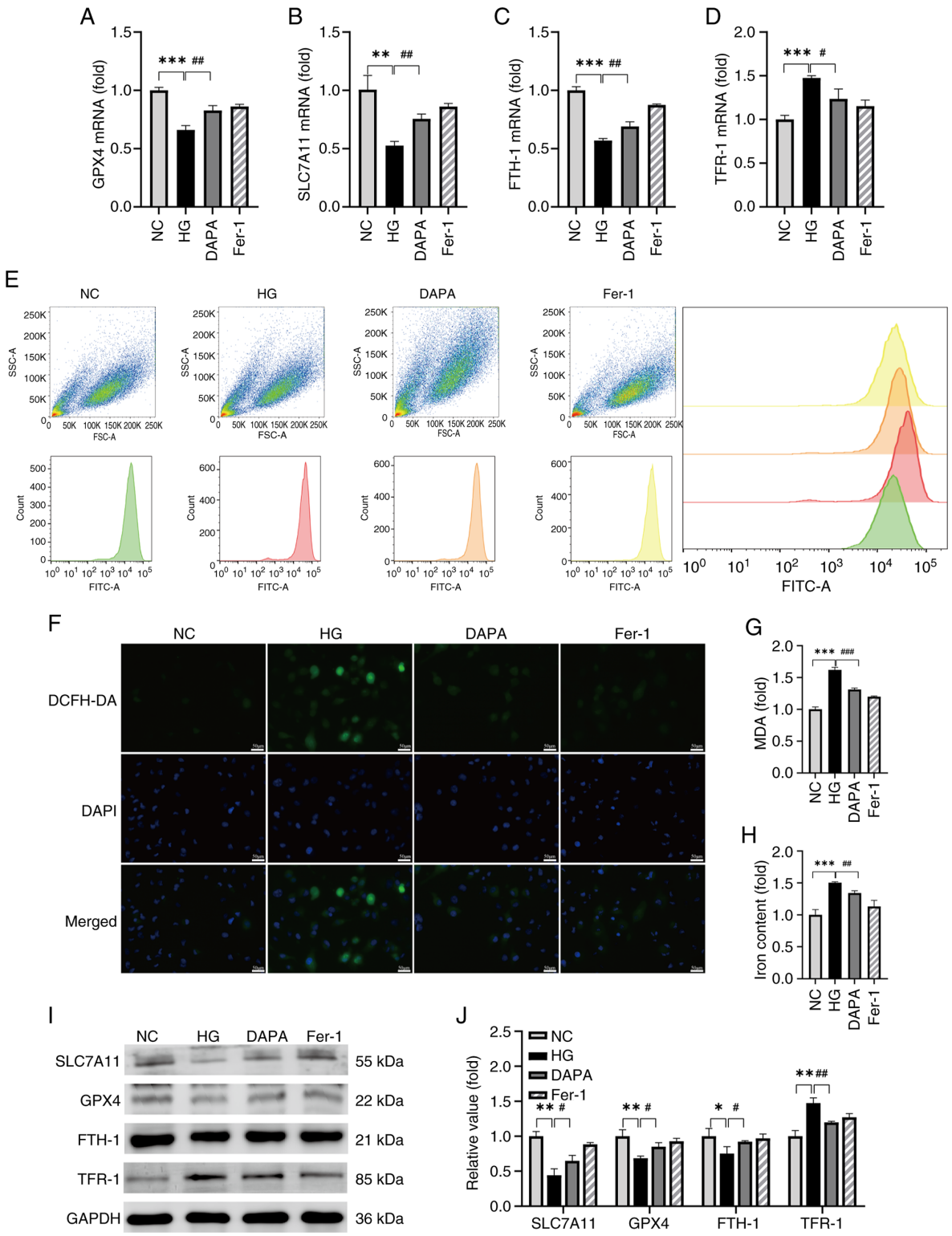

Figure 2. Inhibition of HG-induced ferroptosis in HK-2 cells using DAPA. The mRNA expression levels of (A) GPX4, (B) SLC7A11, (C) FTH-1 and (D) TFR-1 in each cell group were evaluated. (E and F) reactive oxygen species expression, (G) MDA and (H) cellular iron levels were measured in cells from each group. (I) The protein expression levels of SLC7A11, GPX4, FTH-1 and TFR-1 in cells from the NC, HG, DAPA and Fer-1 groups were analyzed. (J) Semi-quantitative analysis of the GPX4, SLC7A11, FTH-1 and TFR-1 immunoblotting results in cells was performed. The bars indicate the mean ± SD from three independent experiments. *P<0.05, **P<0.01, ***P<0.001 compared with the NC group; $^{\#}$P<0.05, $^{\#\#}$P<0.01, $^{\#\#\#}$P<0.001 compared with the HG group. MDA, malondialdehyde; HG, high glucose; NC, normal control; Fer-1, ferrostatin-1; DAPA, dapagliflozin; GPX4, glutathione peroxidase 4; SLC7A11, solute carrier family 7, member 11; FTH-1, ferritin heavy chain 1; TFR-1, transferrin receptor 1.

conducted using a mouse model of type 2 DN. The model was established by feeding male C57BL/6J mice a HFD and administering a low dose of STZ (Fig. 4A). Mice in the NC group exhibited a lively demeanor, glossy fur and consistent patterns in food intake, water consumption and body weight. By contrast, mice in the DN group began displaying symptoms

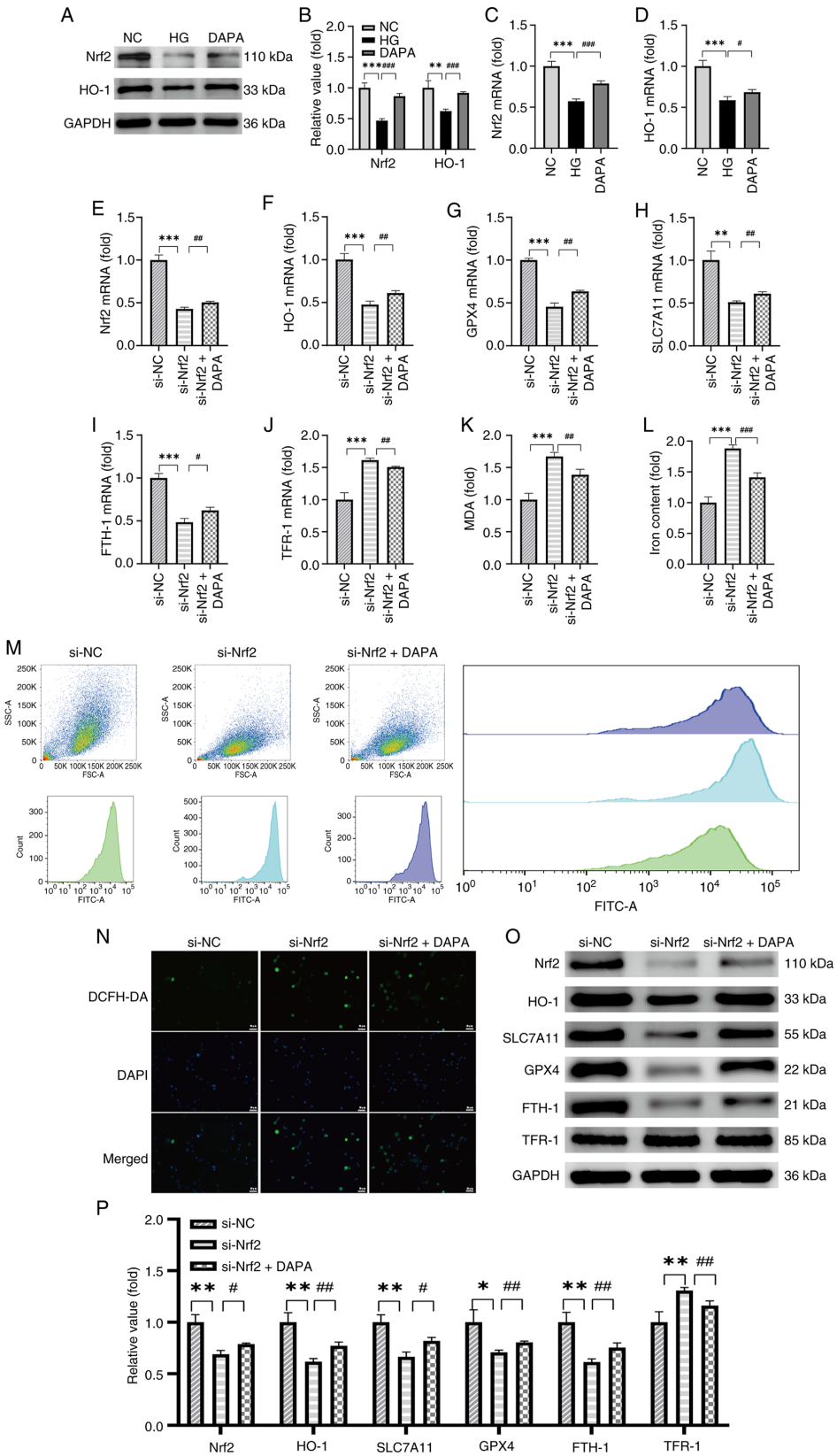

Figure 3. DAPA activates the Nrf2/HO-1 signaling pathway in HG-induced HK-2 cells. (A) The Nrf2 and HO-1 western blotting results in each cell group. (B) Semi-quantitative analysis of the Nrf2 and HO-1 western blotting results in each cell group. The mRNA expression levels of (C) Nrf2 and (D) HO-1 in each cell group were evaluated. The mRNA expression levels of (E) Nrf2, (F) HO-1, (G) GPX4, (H) SLC7A11, (I) FTH-1 and (J) TFR-1 in cells from each group are shown. The (K) MDA and (L) iron content in cells from each group are presented. (M and N) Representative images of reactive oxygen species production in each group, as detected by DCFH-DA staining, are shown. (O) The expression levels of Nrf2, HO-1, GPX4, SLC7A11, FTH-1 and TFR-1 in cells from each group were detected by immunoblotting. (P) Semi-quantitative analysis of protein blot results for Nrf2, HO-1, GPX4, SLC7A11, FTH-1 and TFR-1 in each group is shown. The bars indicate the mean ± SD from three independent experiments. *P<0.05, **P<0.01, ***P<0.001 compared with the HG group; $^{\#}$P<0.05, $^{\#\#}$P<0.01, $^{\#\#\#}$P<0.001 compared with the si-Nrf2 group. DAPA, dapagliflozin; HG, high glucose; NC, normal control; si, small interfering; Nrf2, nuclear factor erythroid2-related factor 2; HO-1, heme oxygenase-1; GPX4, glutathione peroxidase 4; SLC7A11, solute carrier family 7, member 11; FTH-1, ferritin heavy chain 1; TFR-1, transferrin receptor 1; MDA, malondialdehyde; DCFH-DA, 2',7'-dichlorodihydrofluorescein diacetate.

such as increased thirst, appetite and urination, along with weight loss (Fig. 4C-F), and showed lethargy and a dull coat. There was no marked change in blood glucose levels in the normal group of mice. However, after 3 days of STZ injection, random blood glucose levels in the DN, DAPA, si-NC, si-Nrf2 and si-Nrf2 + DAPA groups gradually rose, reaching 23 mmol/l by week 15. Subsequently, the random glucose levels in the DAPA group gradually decreased, while those in the si-Nrf2 + DAPA group began to marginally decline at week 17. By the 23rd week, the random blood glucose levels in the DAPA group approached those of the NC group, and those in the si-Nrf2 + DAPA group approached those of the si-NC group (Fig. 4B), suggesting that DAPA effectively controlled diabetic blood glucose levels. Urinary protein levels serve as an important biomarker for assessing the success of the DN mouse model. The urinary albumin (Fig. 4G), urinary creatinine (Fig. 4H) and ACR (Fig. 4I) showed an increase in the DN group compared with the NC group at week 15. Changes in serum creatinine levels can reflect renal function. The results showed that serum creatinine levels were significantly increased in the DN group and the si-Nrf2 group compared with the DAPA and si-Nrf2 + DAPA groups, respectively (Fig. 4J). These findings suggest that DAPA treatment improved renal function in mice with DN.

DAPA ameliorates ferroptosis and renal pathological injury in DN mice via activation of the Nrf2/HO-1 pathway

Examination of ferroptosis-related parameters in mice. Subsequently, the expression levels of Nrf2, HO-1 and ferroptosis-related markers in the renal tissues of mice from the DN and DAPA groups were evaluated. Results from RT-qPCR and protein blotting analyses revealed significant upregulation of Nrf2 (Fig. 5A and I), HO-1 (Fig. 5B and I), GPX4 (Fig. 5C and I), SLC7A11 (Fig. 5D and I) and FTH-1 (Fig. 5E and I) in the DAPA group compared with the DN group. Additionally, TFR-1 expression was notably decreased in the DAPA group compared with the DN group (Fig. 5F and I). Furthermore, the MDA (Fig. 5G) and iron content (Fig. 5H) levels were significantly reduced in the renal tissues of DAPA-treated mice compared with the DN group, indicating a mitigated ferroptosis phenotype. To further corroborate the protective effect of DAPA on DN kidneys through ferroptosis inhibition via Nrf2/HO-1 upregulation, si-Nrf2 mice were treated with DAPA. Both the mRNA and protein levels of Nrf2 and HO-1 were significantly elevated in the DAPA-treated si-Nrf2 mice compared with the si-Nrf2 group (Fig. 5A, B and I). Additionally, DAPA reversed the altered expression of ferroptosis-related genes at both the mRNA and protein levels: The decreased expression of GPX4, SLC7A11 and FTH-1 in renal tissues of the si-Nrf2 group was improved by DAPA, while the elevated expression of TFR-1 was inhibited by DAPA (Fig. 5C-F and I). Notably, DAPA pretreatment also decreased the MDA (Fig. 5G) and iron content (Fig. 5H), indicating its potential to alleviate iron overload and lipid peroxidation induced by Nrf2 knockdown. Overall, these findings suggest that DAPA may suppress ferroptosis by activating the Nrf2/HO-1 signaling pathway.

Renal histopathological results in mice. Histopathological examination revealed that DAPA mitigated the pathological alterations characterized by glomerular and tubular epithelial damage. PAS staining demonstrated a reduction in the thickening of the glomerular and tubular basement membranes in the DAPA and si-Nrf2 + DAPA groups, while Masson staining indicated a decrease in collagen fiber deposition in the glomeruli and renal interstitium (Fig. 6A and C). Immunohistochemical analysis revealed that treatment with DAPA led to increased expression of Nrf2, HO-1, SLC7A11, GPX4 and FTH-1 as well as decreased expression of TFR-1 compared with the DN group and si-Nrf2 group (Fig. 6B and D). These findings underscored the significant renal protective effects of DAPA in DN mice.

Discussion

DN represents a notable microvascular complication arising from DM, standing as a primary instigator of chronic kidney disease and eventual ESKD. Ferroptosis, a recently characterized mode of cellular death, is intricately interwoven with diverse cellular metabolic pathways encompassing redox homeostasis and iron metabolism (36). Notably, iron overload and hyperglycemia-induced oxidative stress exert marked influence on the pathogenesis and progression of DN (14). Numerous investigations have underscored the intimate association between ferroptosis and DN progression (37,38). Prior research has highlighted the therapeutic potential of DAPA in managing DM and its complications. The multifaceted effects of DAPA encompass glycemic regulation (39), restoration of glomerular function (40) and mitigation of oxidative stress and fibrosis (41). Despite these advancements, the current body of clinical literature exploring the mechanisms linking ferroptosis to DN and the potential therapeutic role of DAPA remains limited. The present study aimed to elucidate these mechanisms, offering novel insights into therapeutic strategies for DN.

Iron metabolism plays a pivotal role in the intricate dynamics of ferroptosis. Intracellular iron homeostasis, encompassing iron uptake, export, utilization and storage, is orchestrated by a cadre of iron metabolism-related genes, including TFR-1 and FTH-1 (42). TFR1, a plasma membrane protein, governs cellular iron uptake by mediating the endocytosis of transferrin-bound iron into the cell (43). FTH-1 plays a crucial role in iron storage by forming an iron carrier complex, ferritin, in conjunction with another protein, Ferritin Light Chain. This complex adeptly sequesters and stores free iron in a non-toxic form within the cell, thereby mitigating free iron levels (44). In situations of intracellular iron overload, Fe^{2+} engages in a Fenton reaction with HO, giving rise to hydroxyl radicals that bind to polyunsaturated fatty acids, initiating lipid peroxidation and culminating in a marked accumulation of ROS. This ROS-induced lipid peroxidation of phospholipid-containing cell membranes generates MDA, inducing cellular oxidative stress and toxicity, ultimately triggering ferroptosis (45). The regulation of ferroptosis primarily revolves around System Xc-, GSH metabolism and the modulation of GPX4 activity. System Xc-comprises SLC3A2 and SLC7A11 dimers integrated into the cell membrane surface, with SLC7A11 being the principal subunit responsible for transporting cystine into the cell for GSH synthesis (46). GSH serves as an essential cofactor for GPX4, which degrades small molecule peroxides and certain lipid peroxides, thus inhibiting

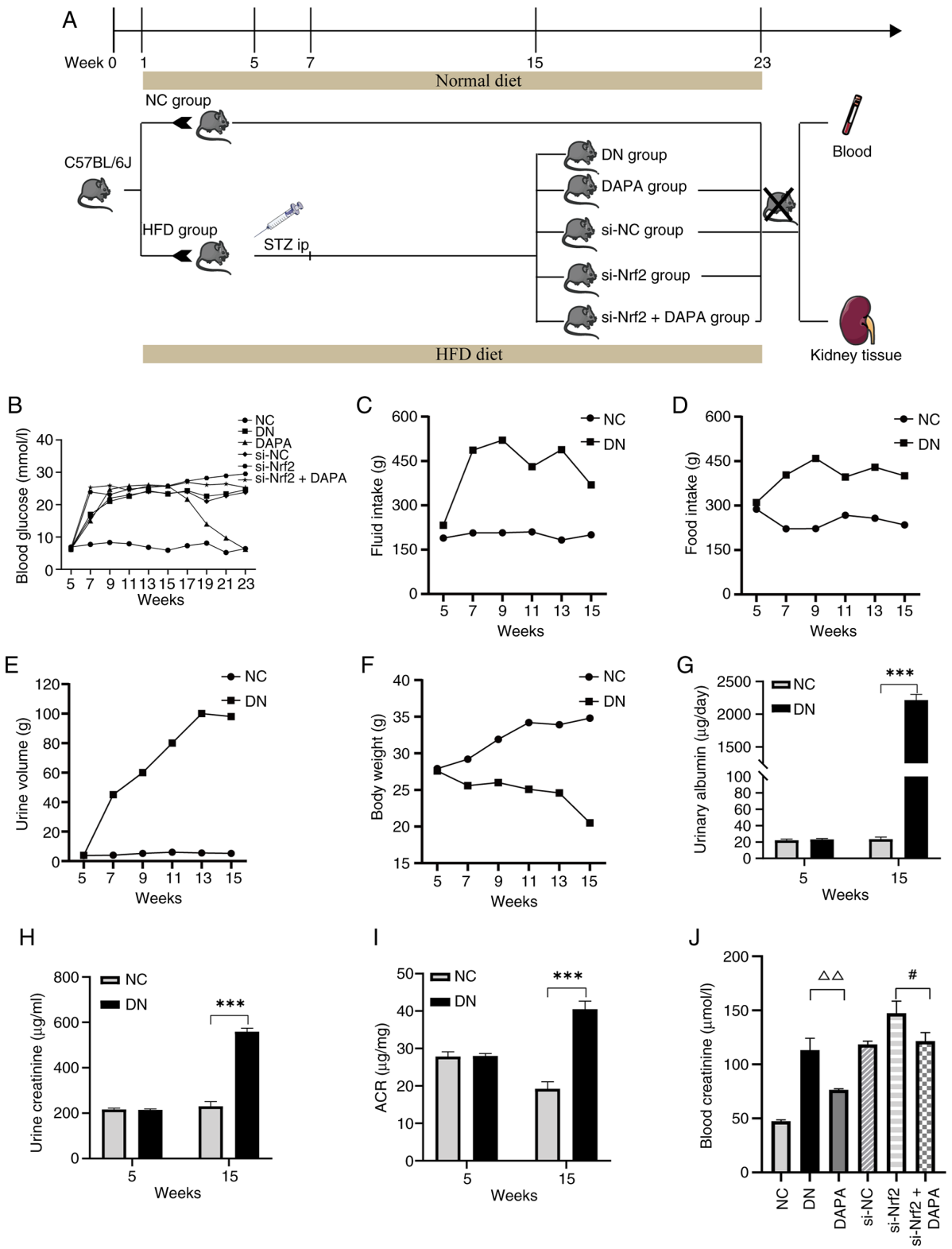

Figure 4. Diabetic nephropathy mouse model. (A) Modeling process of mice with diabetic nephropathy mice. (B) Random blood glucose levels of mice were monitored at weeks 5, 7, 9, 11, 13, 15, 17, 19, 21 and 23. (C) Water intake, (D) food intake, (E) urine output and (F) body weight were measured in mice at weeks 5, 7, 9, 11, 13 and 15. Mice were assayed for (G) 24-h urine albumin level, (H) urine creatinine and (I) ACR at 5 and 15 weeks. (J) Mice were tested for blood creatinine at 23 weeks. The bars indicate the mean ± SD. ***P<0.001 compared with the NC group; $^{\Delta\Delta}$P<0.01 compared with the DN group; $^{\#}$P<0.05 compared with the si-Nrf2 group. NC, normal control; si-NC, si-negative control; DN, diabetic nephropathy; HFD, high-fat diet; STZ, streptozotocin; ip, Intraperitoneal Injection; DAPA, dapagliflozin; si, small interfering; Nrf2, nuclear factor erythroid2-related factor 2; ACR, the urinary albumin-to-creatinine ratio.

lipid peroxidation and serving as a major scavenger of intracellular lipid peroxides. Consequently, inhibition of SLC7A11 and GPX4 expression triggers ferroptosis (47).

In the present study, the expression of ferroptosis-related factors in hyperglycemia-induced HK-2 cells were evaluated as a positive control, with erastin utilized as a reference. The

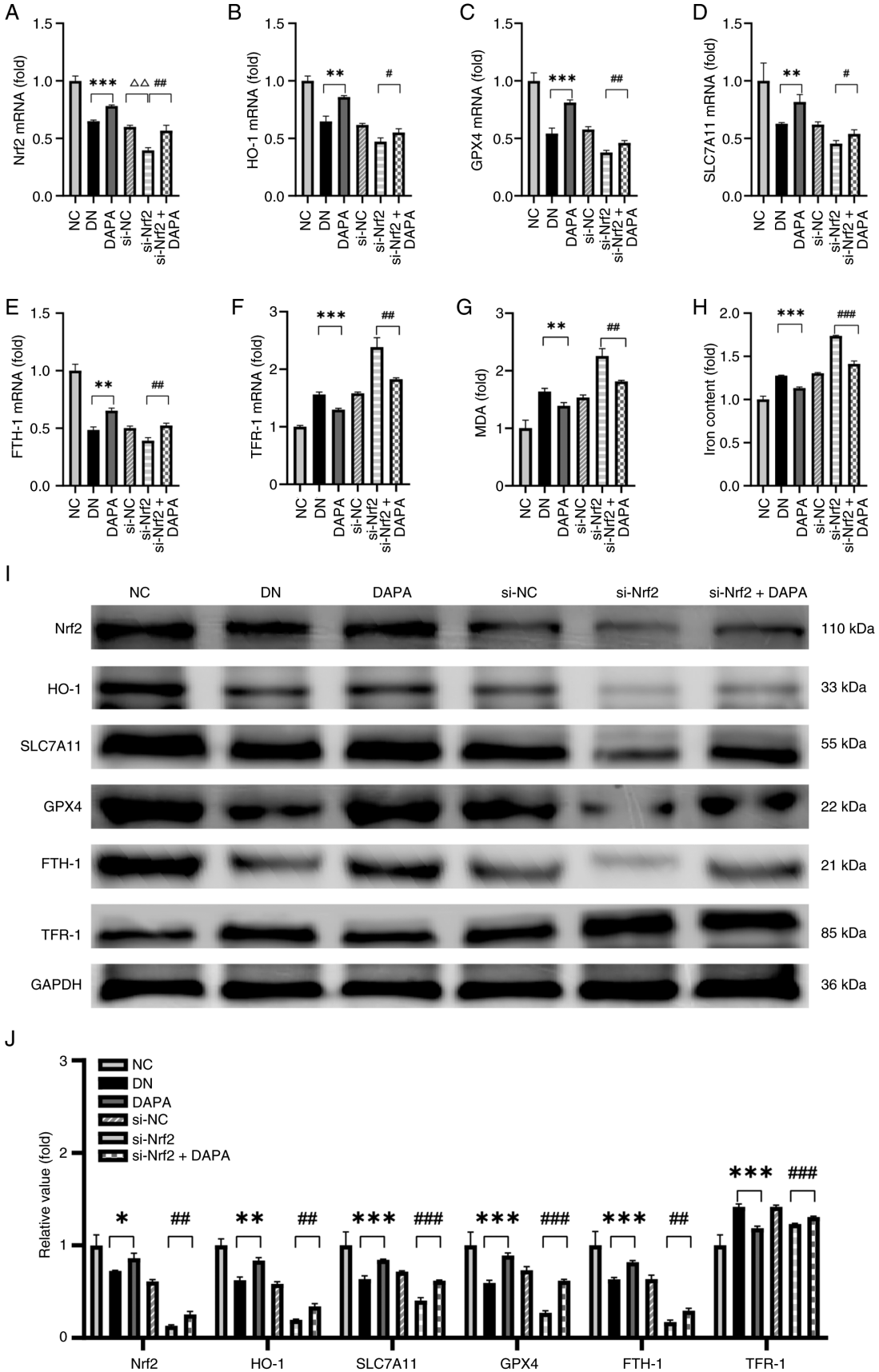

Figure 5. DAPA mitigates ferroptosis in DN mice through activation of the Nrf2/HO-1 pathway. mRNA expression levels of (A) Nrf2, (B) HO-1, (C) GPX4, (D) SLC7A11, (E) FTH-1 and (F) TFR-1 in renal tissues from mice. (G) MDA and (H) iron content measurements in kidney tissue lysates. (I) Western blotting results and (J) semi-quantitative analysis of Nrf2, HO-1, SLC7A11, GPX4, FTH-1 and TFR-1 in mouse kidney tissues. The bars indicate the mean ± SD from three independent experiments. *P<0.05, **P<0.01, ***P<0.001 compared with the DN group; $^{\Delta\Delta}$P<0.01 compared with the si-NC group; $^{\#}$P<0.05, $^{\#\#}$P<0.01, $^{\#\#\#}$P<0.001 compared with the si-Nrf2 group. NC, normal control; si-NC, si-negative control; DN, diabetic nephropathy; DAPA, dapagliflozin; si, small interfering; Nrf2, nuclear factor erythroid2-related factor 2; HO-1, heme oxygenase-1; GPX4, glutathione peroxidase 4; SLC7A11, solute carrier family 7, member 11; FTH-1, ferritin heavy chain 1; TFR-1, transferrin receptor 1; MDA, malondialdehyde.

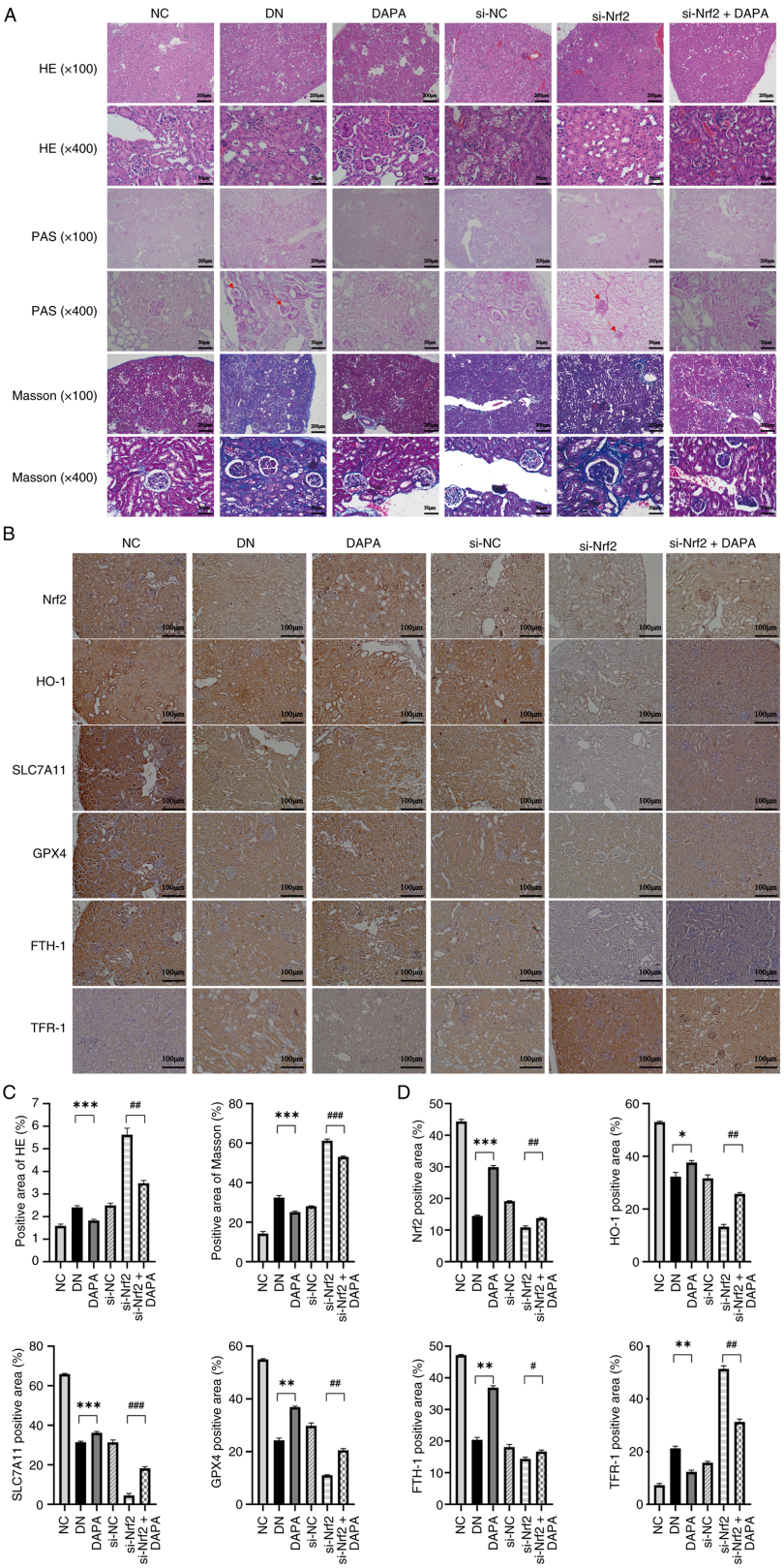

Figure 6. HE, Masson and PAS staining as well as immunohistochemical fluorescence staining. (A) Compared with the DN and si-Nrf2 groups, HE staining showed that the DAPA and si-Nrf2 DAPA groups did not exhibit the pathological alterations characterized by glomerular and tubular epithelial damage. PAS staining demonstrated a reduction in the thickening of glomerular and tubular basement membranes in the DAPA and si-Nrf2 + DAPA groups, while Masson staining indicated a decrease in collagen fiber deposition in the glomeruli and renal interstitium in the DAPA and si-Nrf2 DAPA groups. (B) Immunohistochemical analysis revealed that, compared with the NC and si-NC groups, the DN and si-Nrf2 groups exhibited reduced Nrf2, HO-1, SLC7A11, GPX4 and FTH-1 protein levels, along with elevated TFR-1 expression in renal tissues. However, treatment with DAPA led to increased expression of Nrf2, HO-1, SLC7A11, GPX4 and FTH-1, and decreased expression of TFR-1. (C) Semi-quantitative analysis of HE and Masson staining. (D) Semi-quantitative analysis of the Nrf2, HO-1, SLC7A11, GPX4, FTH-1 and TFR-1 immunohistochemical staining. The bars indicate the mean ± SD from three independent samples. *P<0.05, **P<0.01, ***P<0.001 compared with the DN group; $^{\#}$P<0.05, $^{\#\#}$P<0.01, $^{\#\#\#}$P<0.001 compared with the si-Nrf2 group. DN, diabetic nephropathy; NC, normal control; si, small interfering; Nrf2, nuclear factor erythroid2-related factor 2; HE, hematoxylin and Eosin; DAPA, dapagliflozin; HO-1, heme oxygenase-1; SLC7A11, solute carrier family 7, member 11; GPX4, glutathione peroxidase 4; FTH-1, ferritin heavy chain 1; TFR-1, transferrin receptor 1.

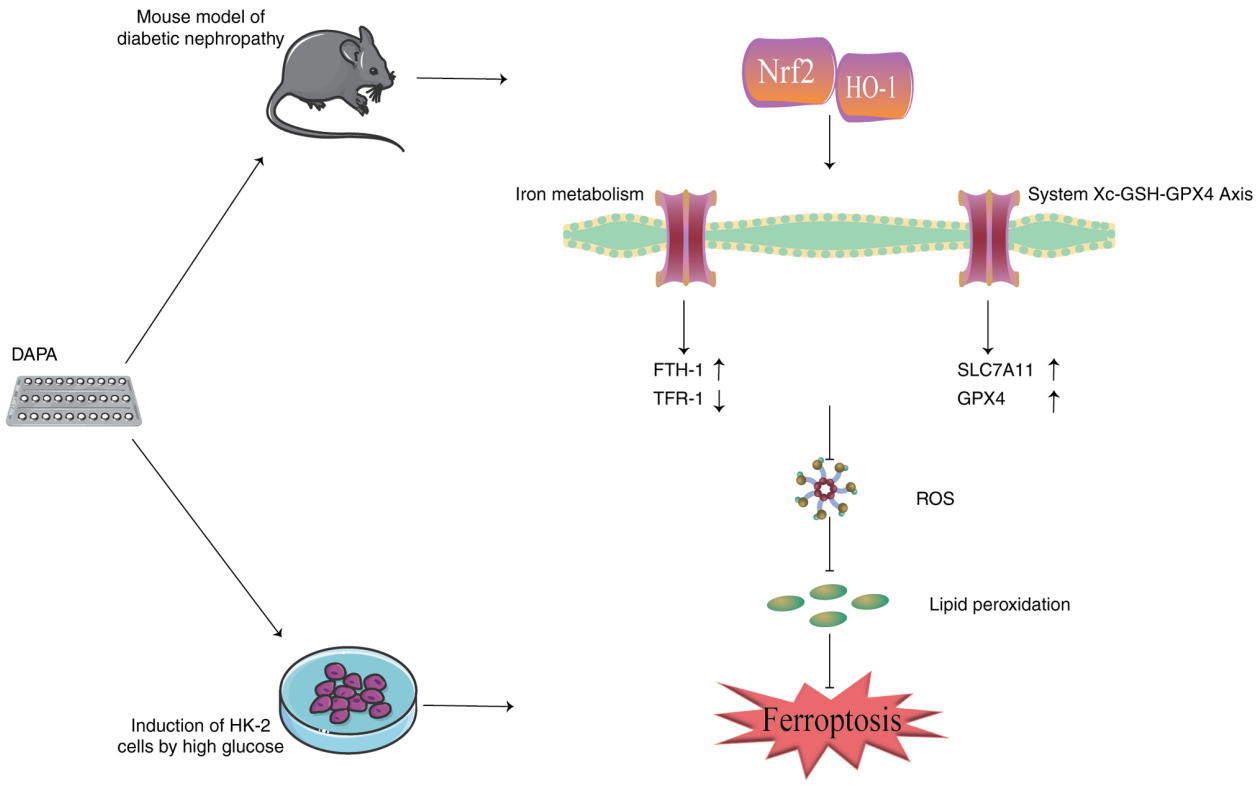

Figure 7. Schematic representation of the mechanism underlying the amelioration of ferroptosis by DAPA. DAPA, dapagliflozin; Nrf2, nuclear factor erythroid2-related factor 2; HO-1, heme oxygenase-1; FTH-1, ferritin heavy chain 1; TRF-1, transferrin receptor 1; SLC7A11, solute carrier family 7, member 11; GPX4, glutathione peroxidase 4; ROS, reactive oxygen species.

findings revealed downregulation of GPX4, SLC7A11 and FTH-1 expression and upregulation of TFR-1 in the renal tissues of DN mice and HG-induced HK-2 cells. Additionally, the levels of ROS expression, iron content and the lipid peroxidation product MDA increased, mirroring the expression patterns following erastin treatment, indicating an association between ferroptosis and DM development. In recent years, the critical role of ferroptosis in the pathogenesis and progression of DM and its complications has been increasingly recognized (48-50), aligning with current understandings (51). Furthermore, ferroptosis has been linked to tubular injury and fibrosis in DN (22,52). Notably, DAPA has been found to potentially mitigate myocardial IRI by inhibiting ferroptosis via the MAPK signaling pathway (53). To delve deeper into whether DAPA shields against DN by impeding ferroptosis, HG-induced HK-2 cells were employed to simulate the DN state and a DN mouse model was established in the present study. The results indicated that DAPA intervention demonstrated a partial reversal of ferroptosis-related factor expression. DN mice showed improved glycemic control and reduced serum creatinine, together with improvements in glomerular morphology, tubular epithelial injury, basement membrane thickening and renal interstitial fibrosis. These findings suggest a protective effect of DAPA on DN, consistent with Huang *et al* (33). Notably, random blood glucose levels have been reported in the present study, which are variable and can be influenced by feeding status and measurement timing. In addition, the high-sugar/HFD + low-dose STZ model utilized typically retains residual β-cell function; therefore, near-normal mean random glucose with SGLT2 inhibition has been reported in STZ-related rodent models (54). A previous study has shown that empagliflozin can alleviate acute tubular injury by mitigating ferroptosis (55). Taken together, the results of the present study support that DAPA may slow DN progression, at least in part, by inhibiting ferroptosis.

Previous investigations have elucidated the role of Nrf2 as a transcription factor pivotal in orchestrating anti-oxidative stress mechanisms (56). Numerous downstream target genes of Nrf2 are instrumental in forestalling or rectifying cellular redox imbalances, thereby playing crucial roles in eliciting antioxidant responses within the organism. Nrf2 comprises seven Neh structural domains, each imbued with distinct functionalities. Among these, the amino-terminal Neh2 domain facilitates interaction with Keap1 is a substrate adaptor protein for the Cullin3 (Cul3)-dependent E3 ubiquitin ligase complex (57). Under normal physiological conditions, the Keap1-Cul3-E3 ubiquitin ligase complex targets multiple lysine residues within the Neh2 domain at the N-terminus of Nrf2 (between the DLG and ETGE motifs), promoting ubiquitination for subsequent degradation. However, under stress conditions, electrophilic reagents and oxidants trigger Nrf2-dependent cellular defense mechanisms, leading to the liberation of Nrf2 from Keap1 and its translocation into the nucleus. Here, it binds to antioxidant-responsive elements, initiating the transcription of various antioxidant genes [such as NAD(P)H:quinone oxidoreductase 1, glutathione S-transferase, heme oxygenase 1, γ-glutamylcysteine ligase and GSH] (58).

HO-1 serves as a principal effector of Nrf2-dependent cellular responses, with HO-1 and its metabolites playing

pivotal roles in maintaining cellular homeostasis (59). It is widely recognized that the Nrf2/HO-1 signaling pathway holds promise as a therapeutic target for combating oxidative stress (60). Moreover, an abundance of prior studies have underscored the protective effects of Nrf2/HO-1 pathway activation against renal oxidative damage in diabetic models (61-63). Based on these findings, we hypothesized that DAPA might impede DN progression through modulation of the Nrf2/HO-1 pathway. The investigations of the present study revealed diminished Nrf2 and HO-1 expression in HG-induced HK-2 cells *in vitro* and in an *in vivo* DN model. However, treatment with DAPA significantly upregulated Nrf2 and HO-1 expression. These findings suggest that DAPA could potentially slow DN progression by activating the Nrf2/HO-1 signaling axis.

In recent years, the Nrf2/HO-1 pathway has emerged as a pivotal player in the progression or prevention of ferroptosis across a spectrum of diseases (such as gastric cancer, neurological diseases, osteoporotic fractures and liver cancer) (64-67). Subsequently, the present study sought to further elucidate the interplay among DAPA, DN and ferroptosis by knocking down Nrf2 expression. The results demonstrated that Nrf2 knockdown led to reduced HO-1 expression, as well as decreased mRNA and protein levels of ferroptosis-related genes. Additionally, Nrf2 knockdown upregulated the ROS, MDA and iron content levels, while the protective role of DAPA in mitigating DN by inhibiting ferroptosis was also somewhat attenuated. Collectively, through the series of *in vivo* and *in vitro* studies outlined above, the findings of the present study suggest that DAPA could delay DN progression by inhibiting ferroptosis through activation of the Nrf2/HO-1 signaling pathway (Fig. 7).

There are several limitations in the present study that should be noted. First, due to the difficulty of obtaining renal tissues from patients with DN, validation of the findings using human samples was not possible. Second, an Nrf2-deficient model generated by gene-editing approaches was not employed, which limits the ability to establish Nrf2 as a necessary mediator of the observed effects *in vivo*. Third, it was not investigated whether DAPA affects the nuclear translocation of Nrf2. Fourth, DN involves multiple regulated cell-death pathways with potential crosstalk, and since apoptosis-related proteins (such as the caspase family) and autophagy markers (such as LC3 and p62) were not assessed, it cannot be excluded that DAPA also modulates these pathways and contributes to the observed protective effects. HG. Fifth, in the HK-2 HG model, an Nrf2-dependent signaling effect of DAPA could not be fully separated from a metabolic contribution related to altered cellular glucose handling and reduced ROS levels, as intracellular glucose uptake or flux were not evaluated. Future studies assessing Keap1 expression, incorporating human samples and using Nrf2-deficient models, together with measurements of apoptosis and autophagy markers, will help strengthen the mechanistic interpretation.

In conclusion, the present study elucidated the occurrence of ferroptosis in HK-2 cells induced by HG and in the renal tissues of mice with DN. Furthermore, the findings suggested that DAPA may attenuate HG-induced ferroptosis and mitigate histological damage and functional abnormalities in the kidneys of diabetic nephropathic mice, both *in vivo* and *in vitro*. These effects may be mediated through the modulation of iron metabolism, the inhibition of lipid peroxidation and the enhancement of antioxidant capacity. Collectively, the present study provides compelling evidence that DAPA may impede the progression of DN by suppressing ferroptosis through activation of the Nrf2/HO-1 signaling pathway.

Acknowledgements

We acknowledge Anhui Province Key Laboratory of Basic and Translational Research of Inflammation-related Diseases for providing the necessary experimental platform, technical support and research environment for this study.

Funding

The present study was supported by the Natural Science Foundation of Anhui Province (grant no. 2208085MH216), the Major Natural Science and Technology Project of Bengbu Medical University (grant no. 2020byfy004), The Scientific Research Program of Anhui Provincial Health Commission (grant no. AHWJ2023BAc10028) and the Bengbu Medical University Graduate Research and Innovation Program Project (grant no. Byycx22019).

Availability of data and materials

The data generated in the present study may be requested from the corresponding author.

Authors' contributions

HL and XH confirm the authenticity of all the raw data. HL participated in the conceptualization, design and implementation of experimental methods, data collection, experimental operations, investigation and organization of related research data and original draft preparation. XZ and YC participated in the design of the experimental methods, data collection, the investigation and organization of related research data and proofreading. SX, LH, ML and CS participated in the collection, verification and organization of research data, as well as careful proofreading and revision of the manuscript. XH participated in supervision, resources, writing, reviewing and editing the manuscript, the overall conception and experimental design of the study, guidance and suggestions in establishing the research ideas, constructing the research framework, refining the key scientific questions and formulating the research plan. All authors read and approved the final version of the manuscript.

Ethics approval and consent to participate

All animal experiments and research procedures were approved by the Clinical Medical Research Ethics Committee of the First Affiliated Hospital of Bengbu Medical University [approval no. (2023) No. 592].

Patient consent for publication

Not applicable.

Competing interests

The authors declare that they have no competing interests.

References

1. Selby NM and Taal MW: An updated overview of diabetic nephropathy: Diagnosis, prognosis, treatment goals and latest guidelines. Diabetes Obes Metab 22 (Suppl 1): S3-S15, 2020.
2. Ashfaq A, Meineck M, Pautz A, Arioglu-Inan E, Weinmann-Menke J and Michel MC: A systematic review on renal effects of SGLT2 inhibitors in rodent models of diabetic nephropathy. Pharmacol Ther 249: 108503, 2023.
3. Luk AO, Li X, Zhang Y, Guo X, Jia W, Li W, Weng J, Yang W, Chan WB, Ozaki R, *et al*: Quality of care in patients with diabetic kidney disease in Asia: The Joint Asia diabetes evaluation (JADE) registry. Diabet Med 33: 1230-1239, 2016.
4. Bays H: From victim to ally: The kidney as an emerging target for the treatment of diabetes mellitus. Curr Med Res Opin 25: 671-681, 2009.
5. Anders HJ, Davis JM and Thurau K: Nephron protection in diabetic kidney disease. N Engl J Med 375: 2096-2098, 2016.
6. Shimizu M, Suzuki K, Kato K, Jojima T, Iijima T, Murohisa T, Iijima M, Takekawa H, Usui I, Hiraishi H and Aso Y: Evaluation of the effects of dapagliflozin, a sodium-glucose co-transporter-2 inhibitor, on hepatic steatosis and fibrosis using transient elastography in patients with type 2 diabetes and non-alcoholic fatty liver disease. Diabetes Obes Metab 21: 285-292, 2019.
7. Diaz-Cruz C, Gonzalez-Ortiz M, Rosales-Rivera LY, Patino-Laguna AJ, Ramirez-Rodriguez ZG, Diaz-Cruz K and Martínez-Abundis E: Effects of dapagliflozin on blood pressure variability in patients with prediabetes and prehypertension without pharmacological treatment: A randomized trial. Blood Press Monit 25: 346-350, 2020.
8. Xin Y, Guo Y, Li Y, Ma Y, Li L and Jiang H: Effects of sodium glucose cotransporter-2 inhibitors on serum uric acid in type 2 diabetes mellitus: A systematic review with an indirect comparison meta-analysis. Saudi J Biol Sci 26: 421-446, 2019.
9. Jhund PS, Ponikowski P, Docherty KF, Gasparyan SB, Bohm M, Chiang CE, Desai AS, Howlett J, Kitakaze M, Petrie MC, *et al*: Dapagliflozin and recurrent heart failure hospitalizations in heart failure with reduced ejection fraction: An analysis of DAPA-HF. Circulation 143: 1962-1972, 2021.
10. McMurray JJV, Wheeler DC, Stefansson BV, Jongs N, Postmus D, Correa-Rotter R, Chertow GM, Greene T, Held C, Hou FF, *et al*: Effect of dapagliflozin on clinical outcomes in patients with chronic kidney disease, with and without cardiovascular disease. Circulation 143: 438-448, 2021.
11. Wiviott SD, Raz I, Bonaca MP, Mosenzon O, Kato ET, Cahn A, Silverman MG, Zelniker TA, Kuder JF, Murphy SA, *et al*: Dapagliflozin and cardiovascular outcomes in type 2 diabetes. N Engl J Med 380: 347-357, 2019.
12. Heerspink HJL, Stefansson BV, Chertow GM, Correa-Rotter R, Greene T, Hou FF, Lindberg M, McMurray J, Rossing P, Toto R, *et al*: Rationale and protocol of the dapagliflozin and prevention of adverse outcomes in chronic kidney disease (DAPA-CKD) randomized controlled trial. Nephrol Dial Transplant 35: 274-282, 2020.
13. Quagliariello V, De Laurentiis M, Rea D, Barbieri A, Monti MG, Carbone A, Paccone A, Altucci L, Conte M, Canale ML, *et al*: The SGLT-2 inhibitor empagliflozin improves myocardial strain, reduces cardiac fibrosis and pro-inflammatory cytokines in non-diabetic mice treated with doxorubicin. Cardiovasc Diabetol 20: 150, 2021.
14. Dixon SJ, Lemberg KM, Lamprecht MR, Skouta R, Zaitsev EM, Gleason CE, Patel DN, Bauer AJ, Cantley AM, Yang WS, *et al*: Ferroptosis: An iron-dependent form of nonapoptotic cell death. Cell 149: 1060-1072, 2012.
15. Yang XD and Yang YY: Ferroptosis as a novel therapeutic target for diabetes and its complications. Front Endocrinol (Lausanne) 13: 853822, 2022.
16. Stockwell BR: Ferroptosis turns 10: Emerging mechanisms, physiological functions, and therapeutic applications. Cell 185: 2401-2421, 2022.
17. Kajarabille N and Latunde-Dada GO: Programmed Cell-death by ferroptosis: Antioxidants as mitigators. Int J Mol Sci 20: 4968, 2019.
18. Ayala A, Munoz MF and Arguelles S: Lipid peroxidation: Production, metabolism, and signaling mechanisms of malondialdehyde and 4-hydroxy-2-nonenal. Oxid Med Cell Longev 2014: 360438, 2014.
19. Li S, Zheng L, Zhang J, Liu X and Wu Z: Inhibition of ferroptosis by up-regulating Nrf2 delayed the progression of diabetic nephropathy. Free Radic Biol Med 162: 435-449, 2021.
20. Lee H, Zandkarimi F, Zhang Y, Meena JK, Kim J, Zhuang L, Tyagi S, Ma L, Westbrook TF, Steinberg GR, *et al*: Energy-stress-mediated AMPK activation inhibits ferroptosis. Nat Cell Biol 22: 225-234, 2020.
21. Muller T, Dewitz C, Schmitz J, Schroder AS, Brasen JH, Stockwell BR, Murphy JM, Kunzendorf U and Krautwald S: Necroptosis and ferroptosis are alternative cell death pathways that operate in acute kidney failure. Cell Mol Life Sci 74: 3631-3645, 2017.
22. Wang Y, Bi R, Quan F, Cao Q, Lin Y, Yue C, Cui X, Yang H, Gao X and Zhang D: Ferroptosis involves in renal tubular cell death in diabetic nephropathy. Eur J Pharmacol 888: 173574, 2020.
23. Zhang L, Zhang J, Jin Y, Yao G, Zhao H, Qiao P and Wu S: Nrf2 is a potential modulator for orchestrating iron homeostasis and redox balance in cancer cells. Front Cell Dev Biol 9: 728172, 2021.
24. Parfenova H, Basuroy S, Bhattacharya S, Tcheranova D, Qu Y, Regan RF and Leffler CW: Glutamate induces oxidative stress and apoptosis in cerebral vascular endothelial cells: Contributions of HO-1 and HO-2 to cytoprotection. Am J Physiol Cell Physiol 290: C1399-C1410, 2006.
25. Garcia-Nino WR and Pedraza-Chaverri J: Protective effect of curcumin against heavy metals-induced liver damage. Food Chem Toxicol 69: 182-201, 2014.
26. Lu C, Xu W, Zhang F, Shao J and Zheng S: Nrf2 knockdown disrupts the protective effect of curcumin on Alcohol-induced hepatocyte necroptosis. Mol Pharm 13: 4043-4053, 2016.
27. Lu C, Zhang F, Xu W, Wu X, Lian N, Jin H, Chen Q, Chen L, Shao J, Wu L, *et al*: Curcumin attenuates ethanol-induced hepatic steatosis through modulating Nrf2/FXR signaling in hepatocytes. IUBMB Life 67: 645-658, 2015.
28. Han L, Li L and Wu G: Induction of ferroptosis by carnosic acid-mediated inactivation of Nrf2/HO-1 potentiates cisplatin responsiveness in OSCC cells. Mol Cell Probes 64: 101821, 2022.
29. Hu Q, Zuo T, Deng L, Chen S, Yu W, Liu S, Liu J, Wang X, Fan X and Dong Z: β-Caryophyllene suppresses ferroptosis induced by cerebral ischemia reperfusion via activation of the NRF2/HO-1 signaling pathway in MCAO/R rats. Phytomedicine 102: 154112, 2022.
30. Yang W, Wang Y, Zhang C, Huang Y, Yu J, Shi L, Zhang P, Yin Y, Li R and Tao K: Maresin1 protect against ferroptosis-induced liver injury through ROS inhibition and Nrf2/HO-1/GPX4 activation. Front Pharmacol 13: 865689, 2022.
31. Gong F, Ge T, Liu J, Xiao J, Wu X, Wang H, Zhu Y, Xia D and Hu B: Trehalose inhibits ferroptosis via NRF2/HO-1 pathway and promotes functional recovery in mice with spinal cord injury. Aging (Albany NY) 14: 3216-3232, 2022.
32. Yang J, Mo J, Dai J, Ye C, Cen W, Zheng X, Jiang L and Ye L: Cetuximab promotes RSL3-induced ferroptosis by suppressing the Nrf2/HO-1 signalling pathway in KRAS mutant colorectal cancer. Cell Death Dis 12: 1079, 2021.
33. Huang B, Wen W and Ye S: Dapagliflozin ameliorates renal tubular ferroptosis in diabetes via SLC40A1 stabilization. Oxid Med Cell Longev 2022: 9735555, 2022.
34. Zhang Z, Li L, Dai Y, Lian Y, Song H, Dai X, Su R, Yin J and Gu R: Dapagliflozin inhibits ferroptosis and ameliorates renal fibrosis in diabetic C57BL/6J mice. Sci Rep 15: 7117, 2025.
35. Livak KJ and Schmittgen TD: Analysis of relative gene expression data using real-time quantitative PCR and the 2(-Delta Delta C(T)) method. Methods 25: 402-408, 2001.
36. Stockwell BR, Friedmann Angeli JP, Bayir H, Bush AI, Conrad M, Dixon SJ, Fulda S, Gascón S, Hatzios SK, Kagan VE, *et al*: Ferroptosis: A regulated cell death nexus linking metabolism, redox biology, and disease. Cell 171: 273-285, 2017.
37. Tiwari BK, Pandey KB, Abidi AB and Rizvi SI: Markers of oxidative stress during diabetes mellitus. J Biomark 2013: 378790, 2013.
38. Bruni A, Pepper AR, Pawlick RL, Gala-Lopez B, Gamble AF, Kin T, Seeberger K, Korbutt GS, Bornstein SR, Linkermann A and Shapiro AMJ: Ferroptosis-inducing agents compromise in vitro human islet viability and function. Cell Death Dis 9: 595, 2018.

39. Dekkers CCJ, Wheeler DC, Sjostrom CD, Stefansson BV, Cain V and Heerspink HJL: Effects of the sodium-glucose co-transporter 2 inhibitor dapagliflozin in patients with type 2 diabetes and Stages 3b-4 chronic kidney disease. Nephrol Dial Transplant 33: 2005-2011, 2018.
40. Yao D, Wang S, Wang M and Lu W: Renoprotection of dapagliflozin in human renal proximal tubular cells via the inhibition of the high mobility group box 1-receptor for advanced glycation end products-nuclear factor-kappaB signaling pathway. Mol Med Rep 18: 3625-3630, 2018.
41. Oraby MA, El-Yamany MF, Safar MM, Assaf N and Ghoneim HA: Dapagliflozin attenuates early markers of diabetic nephropathy in fructose-streptozotocin-induced diabetes in rats. Biomed Pharmacother 109: 910-920, 2019.
42. Dixon SJ and Stockwell BR: The role of iron and reactive oxygen species in cell death. Nat Chem Biol 10: 9-17, 2014.
43. Xiao C, Fu X, Wang Y, Liu H, Jiang Y, Zhao Z and You F: Transferrin receptor regulates malignancies and the stemness of hepatocellular carcinoma-derived cancer stem-like cells by affecting iron accumulation. PLoS One 15: e0243812, 2020.
44. Zheng J and Conrad M: The metabolic underpinnings of ferroptosis. Cell Metab 32: 920-937, 2020.
45. Sha W, Hu F, Xi Y, Chu Y and Bu S: Mechanism of ferroptosis and its role in type 2 diabetes mellitus. J Diabetes Res 2021: 9999612, 2021.
46. Dodson M, Castro-Portuguez R and Zhang DD: NRF2 plays a critical role in mitigating lipid peroxidation and ferroptosis. Redox Biol 23: 101107, 2019.
47. Yang WS, Kim KJ, Gaschler MM, Patel M, Shchepinov MS and Stockwell BR: Peroxidation of polyunsaturated fatty acids by lipoxygenases drives ferroptosis. Proc Natl Acad Sci USA 113: E4966-E4975, 2016.
48. Hao L, Mi J, Song L, Guo Y, Li Y, Yin Y and Zhang C: SLC40A1 mediates ferroptosis and cognitive dysfunction in type 1 diabetes. Neuroscience 463: 216-226, 2021.
49. Matsumoto M, Sasaki N, Tsujino T, Akahori H, Naito Y and Masuyama T: Iron restriction prevents diabetic nephropathy in Otsuka Long-Evans tokushima fatty rat. Ren Fail 35: 1156-1162, 2013.
50. Wang N, Ma H, Li J, Meng C, Zou J, Wang H, Liu K, Liu M, Xiao X, Zhang H and Wang K: HSF1 functions as a key defender against palmitic acid-induced ferroptosis in cardiomyocytes. J Mol Cell Cardiol 150: 65-76, 2021.
51. Gao HQ, Xu SD, Ren CW, Yang S, Liu CL, Zhen J, Liu YM, Zhu JM, Huang LJ and Sun LZ: Analysis of perioperative outcome and long-term survival rate of thoracic endovascular aortic repair in uncomplicated type B dissection: Single-centre experience with 751 patients. Eur J Cardiothorac Surg 56: 1090-1096, 2019.
52. Feng X, Wang S, Sun Z, Dong H, Yu H, Huang M and Gao X: Ferroptosis enhanced diabetic renal tubular injury via HIF-1alpha/HO-1 Pathway in db/db Mice. Front Endocrinol (Lausanne) 12: 626390, 2021.
53. Chen W, Zhang Y, Wang Z, Tan M, Lin J, Qian X, Li H and Jiang T: Dapagliflozin alleviates myocardial ischemia/reperfusion injury by reducing ferroptosis via MAPK signaling inhibition. Front Pharmacol 14: 1078205, 2023.
54. Pennig J, Scherrer P, Gissler MC, Anto-Michel N, Hoppe N, Funer L, Härdtner C, Stachon P, Wolf D, Hilgendorf I, *et al*: Glucose lowering by SGLT2-inhibitor empagliflozin accelerates atherosclerosis regression in hyperglycemic STZ-diabetic mice. Sci Rep 9: 17937, 2019.
55. Ema C, Iwakura T, Tsuji N, Nakayama Y, Tsuchida M, Kitamura A, Katahashi N, Ishigaki S, Isobe S, Fujikura T, *et al*: Teneligliptin and empagliflozin attenuate ferroptosis-mediated acute tubular injury. Nephrol Dial Transplant 4: 750-765, 2025.
56. Ngo V and Duennwald ML: Nrf2 and oxidative stress: A general overview of mechanisms and implications in human disease. Antioxidants (Basel) 11: 2345, 2020.
57. Kobayashi A, Kang MI, Watai Y, Tong KI, Shibata T, Uchida K and Yamamoto M: Oxidative and electrophilic stresses activate Nrf2 through inhibition of ubiquitination activity of Keap1. Mol Cell Biol 26: 221-229, 2006.
58. Osburn WO and Kensler TW: Nrf2 signaling: An adaptive response pathway for protection against environmental toxic insults. Mutat Res 659: 31-39, 2008.
59. Na HK and Surh YJ: Oncogenic potential of Nrf2 and its principal target protein heme oxygenase-1. Free Radic Biol Med 67: 353-365, 2014.
60. Zhang R, Xu M, Wang Y, Xie F, Zhang G and Qin X: Nrf2-a promising therapeutic target for defensing against oxidative stress in stroke. Mol Neurobiol 54: 6006-6017, 2017.
61. de Haan JB: Nrf2 activators as attractive therapeutics for diabetic nephropathy. Diabetes 60: 2683-2684, 2011.
62. Jiang T, Huang Z, Lin Y, Zhang Z, Fang D and Zhang DD: The protective role of Nrf2 in streptozotocin-induced diabetic nephropathy. Diabetes 59: 850-860, 2010.
63. Wang H, Yu X, Liu D, Qiao Y, Huo J, Pan S, Zhou L, Wang R, Feng Q and Liu Z: VDR activation attenuates renal tubular epithelial cell ferroptosis by regulating Nrf2/HO-1 signaling pathway in diabetic nephropathy. Adv Sci (Weinh) 11: e2305563, 2023.
64. Kong W, Liu X, Zhu H, Zheng S, Yin G, Yu P, Shan Y, Ma S, Ying R and Jin H: Tremella fuciformis polysaccharides induce ferroptosis in Epstein-Barr virus-associated gastric cancer by inactivating NRF2/HO-1 signaling. Aging (Albany NY) 16: 1767-1780, 2024.
65. Qian Z, Zhang Q, Li P, Li Y, Zhang Y, Li R, Zhao T, Xia M, Chen Y and Hong X: A disintegrin and metalloproteinase-8 protects against Erastin-Induced neuronal ferroptosis via activating Nrf2/HO-1/FTH1 signaling pathway. Mol Neurobiol 61: 3490-3502, 2024.
66. Xiang S, Zhao L, Tang C, Ling L, Xie C, Shi Y, Liu W, Li X and Cao Y: Icariin inhibits osteoblast ferroptosis via Nrf2/HO-1 signaling and enhances healing of osteoporotic fractures. Eur J Pharmacol 965: 176244, 2023.
67. Yang R, Gao W, Wang Z, Jian H, Peng L, Yu X, Xue P, Peng W, Li K and Zeng P: Polyphyllin I induced ferroptosis to suppress the progression of hepatocellular carcinoma through activation of the mitochondrial dysfunction via Nrf2/HO-1/GPX4 axis. Phytomedicine 122: 155135, 2024.